9th International Conference on Numerical Ship Hydrodynamics
Ann Arbor, Michigan, August 5-8, 2007

Computation of Forces and Moments of Undersea Vehicles with Non-Body-Of-Revolution Hull

Young S. Hong (Naval Surface Warfare Center,
Carderock Division, U.S.A.

ABSTRACT

The hydrodynamic forces and moments acting on undersea vehicles with non-body-of-revolution hull forms moving in deep water have been computed using a panel method. The method of using a distribution of source singularities is applied to compute forces and moments on the body. The separation angles in the cross-flow direction are assumed to be known. The computed forces and moments are compared with available experimental data. The agreement between the computation and experiment is very good.

INTRODUCTION

A new method to compute the forces and moments for a non-body-of-revolution hull moving with an angle of attack is developed. The velocity distribution on the body surface is calculated with a computer program based on a three-dimensional panel method. The separation angles in the cross-flow direction are assumed to be known. It is also assumed that the pressures in the separated region are the same as that on the surface element where the separation occurs in the cross-flow direction.

A similar method based on a two-dimensional approach is applied to compute forces and moments for the bodies of revolution presented by Hong (1991). The predicted forces and moments for the bodies of various ratios of the length to diameter agree very well with the captive-model test data. The line of separation angle along the length is determined by trial and error from the test data of a spheroid with a length to diameter ratio of 6 for an angle of attack of 30 degrees as presented by Meier et al (1979). The line of separation angle on the blunt body is a function of the Reynolds number, the ratio of length to diameter, the body shape, and the angle of attack among other independent variables. Since there is not much information about the separation line on the blunt body available, the separation line on the non-body-of-revolution hulls is found through a trial-and-error method.

The computed forces and moments of an undersea vehicle, of which the cross section is square with rounded corners, agree very well with the experimental data.

COMPUTATION OF PRESSURE ON THE BODY

There are two coordinate systems: one is oxyz and the other is $o_1x_1y_1z_1$. The coordinate system, oxyz moves at a speed of U, which is the mean speed of the body along the positive ox-axis. The positive oz-axis is directed vertically upwards. The origin, o is located at the free surface above the center of gravity of the body. The coordinate system, $o_1x_1y_1z_1$ located at the center of gravity of the body moves at a speed of U parallel to the free surface and the positive o_1z_1-axis is directed perpendicularly downwards to the o_1x_1-axis as shown in Figure 1. The velocity potential, velocity, and pressure are expressed in the coordinate system, oxyz and later the final forces and moments are converted into the coordinate system, $o_1x_1y_1z_1$. The total velocity potential can be expressed in the oxyz coordinate system as

$$\Phi(x,y,z) = \phi_o(x,y,z) + \phi(x,y,z) \quad (1)$$

where ϕ is the disturbance velocity potential due to the body. The gradient of ϕ_o is given as

$$\nabla\phi_o = (-U,0,0) \quad (2)$$

The disturbance velocity potential ϕ can be expressed in integral form as

$$\phi(x,y,z) = \frac{1}{4\pi}\iint_S G(P,Q)\sigma(Q)dS(Q) \quad (3)$$

where P(x,y,z) is the field point, $Q(x_o,y_o,z_o)$ the source point, S the body surface, σ the unknown strength of sources and sinks distributed on the body surface, and G is the Green function which is given as

$$G(P,Q) = \frac{1}{r} \quad (4)$$

where

$$r^2 = (x-x_o)^2 + (y-y_o)^2 + (z-z_o)^2 \quad (5)$$

The unknown strength of sources and sinks, σ is determined by the body boundary condition, which is

$$\frac{\partial}{\partial n}[\frac{1}{4\pi}\iint G(P,Q)\sigma(Q)dS(Q)] = -\nabla\phi_o \bullet \vec{n} \quad (6)$$

The force acting on the body is expressed as

$$\vec{F} = \iint_S p\vec{n}dS \quad (7)$$

where $\vec{n}$ is the unit normal vector at the body surface. The pressure around the body, p is

$$p = \frac{\rho}{2}[|\nabla\Phi|^2 - |\nabla\phi_o|^2] \quad (8)$$

where ρ is the density of the fluid. The detailed procedure of the numerical solution of Equation (6) is given by Hess and Smith (1962) and Hong (1991).

PRESSURE IN THE SEPARATED REGION

The pressure on the body surface in Equation (8) is used to compute the pressure before the flow separation. Once the flow separates from the body, the pressure in the separated region is the same as the pressure at the surface element where the separation occurs in the cross-flow direction. This indicates that the pressure in the separated region is constant in the cross-flow direction. However, the pressure in the separated region is not constant along the body length. The force acting on the body is modified as follows:

$$\vec{F} = \iint_{S_1} p\vec{n}dS + \iint_{S_2} p_s\vec{n}dS \quad (9)$$

where p_s is the pressure in the separated region, S_1 is the body surface in attached flow, and S_2 is the body surface in the separated region.

TWO-DIMENSIONAL SEPARATION ANGLES IN CROSSFLOW DIRECTION

One of the most difficult tasks in the present study was to determine the location of the separation line on the surface of the body. The hydrodynamic forces and moments developed on the body can not be predicted without knowing the location of the separation line accurately. The location of the separation line is a function of the Reynolds number, angle of attack, and geometry of the body among other independent variables. The measured separation angles of a spheroid are shown in Figure 2 from Reference 2 for the angle of attack of 30 degrees. At the bow the separation angle is about 150 degrees and at the stern the separation angle is 80 degrees. The previous study by Hong (1991) shows that the separation angles of the body of revolution were found to be 170 degrees at the bow and 110 degrees at the stern for all angles of attack and for the fineness ratios between 4 and 12.4.

Since the separation angles are not available analytically or experimentally, it was attempted to determine the separation angle of the non-body-of-revolution hull by a trial-and-error method. The separation angles in the cross flow direction along the length are adjusted until the predicted forces and moments agree with the experimental data. The separation angles are also dependent on the number of panels on the body surface. Since there is not much information about the line of separation on the non-body-of-revolution hulls available, for the present study it is assumed that the separation angles at the bow and stern are the same as those for the body of revolution. The separation angle at the bow for the body of revolution is 170 degrees and that at the stern is 110 degrees. The values of separation angles of 170 and 110 degrees might be good for the body with a pointed stern. If the stern has a finite width, the most aft end of the body might be acting as a lifting surface. In this case the method of a source singularity cannot be applied to compute the forces and moments of blunt bodies.

NUMERICAL RESULTS

The forces and moments are computed for four models, of which principal dimensions are given in Table 1. For the UUV, a non-body-of-revolution hull, and SUBOFF, a body of revolution, there are experimental data available and for non-body-of-revolution hulls, CFF1 and CFF2, no experimental data are available. CFF1 is a body with elliptical section, of which the ratio of the major axis to minor axis is 1.5. CFF2 is a body with elliptical section, of which the ratio of major axis to minor axis is 0.67. Both CFF1 and CFF2 are created from SUBOFF by taking the same length and volume. The discretized body surfaces are plotted in Figure 3. The number of the discretized body surfaces is 2880 for all models. In the labels of the figures, the letter, T indicates the experimental data and the notations are given at the end of this section.

The body surface of an undersea vehicle (UUV), of which the cross section is square with rounded corners, is discretized as shown in Figure 3. The separation angle is 170 degrees at the bow and 110 degrees at the stern. The separation angle at any section is linearly interpolated. The computed forces and moments of this vehicle, which is moving with an angle of attack, α, are compared with the test data in Figure 4. The agreement between the prediction and test is very good. The experiment was performed by Roddy et al (1993). To study the sensitivity of the separation angles at the bow and stern, the forces and moments for two different separation angles are compared with those for the separation angles of 170 degrees at the bow and 110 degrees at the stern. Figure 5 shows the results for the different separation angles at the bow, while the separation angle at the stern is kept as 110 degrees. For the separation angle at the bow of 160 degrees, the forces are computed much larger than those for 170 degrees. The moments are computed almost the same as those for 170 degrees. When the separation angle at the bow is 180 degrees, the forces are computed much smaller than those for 170 degrees. In this case the moments are computed slightly larger than those for 170 degrees. Figure 6 shows the results for the different separation angles at the stern, while the separation angle at the bow is kept as 170 degrees. The forces for the separation angle of 100 degrees are computed much larger than those for the separation angle of 110 degrees and the moments for the separation angle of 100 degrees are computed smaller than those for the separation angle of 110 degrees. When the separation angle is 120 degrees, the forces are computed much smaller and the moments are computed larger than those for the separation angle of 110 degrees. The change of 10 degrees in the separation angles at the bow and stern results in much different forces as shown in

Figures 5 and 6. The results of moment show less sensitivity in the change of the separation angle at the bow. However, the moments are dependent on the separation angle at the stern as shown in Figures 5 and 6. This indicates that the elements at the separation angles of 170 degrees at the bow and 110 degrees at the stern. The forces and moments for the surface elements of 2400 and 3360 are compared with those for 2880. Since the number of surface elements is over 2400, the forces and moments are not highly dependent on the number of surface elements.

Since experimental data is not available for other non-body-of-revolution hulls, two non-body-of-revolution with elliptical sections are created from SUBOFF. SUBOFF is a body of revolution and the experiment was performed by Roddy (1990). The study of the body with the elliptical sections is to investigate the change of the forces and moments depending on the shape of the body. The computed forces and moments of SUBOFF are compared with the experimental data as shown in Figure 8. The separation angles at the bow and stern are 170 and 110 degrees, respectively. The agreement between the prediction and experiment is excellent. The computed forces and moments of CFF1, which is a flat body, are compared with those of SUBOFF as shown in Figure 9. The separation angles at the bow and stern are 170 and 110 degrees, respectively. The forces are computed much smaller than those of SUBOFF and the moments are computed much larger than those of SUBOFF. Since CFF1 is a flat body, the difference in the pressures at the top and bottom surface is smaller than that of the body of revolution and therefore, the forces are computed smaller than those of SUBOFF. If the body thickness becomes very small, then the present panel method computes the pressures at the top and bottom surface almost the same. The results of CFF2 are compared with those of SUBOFF in Figure 10. The separation angles are 170 degrees at the bow and 110 degrees at the stern. In this case the forces are computed the same as those of SUBOFF and the moments are computed much smaller than those of SUBOFF. Since CFF2 is a slender body, the difference in the pressures at the top and bottom surfaces is much larger than that of SUBOFF. The results of Figures 9 and 10 indicate that when the body of revolution becomes a flat body, the forces become smaller and the moments become larger than those of the body of revolution with the same separation angles. The opposite is true when the body of revolution becomes a slender body. Since an experiment is not done for CFF1 and CFF2, it is not possible to validate the present method.

The following notations are used in the figures:

$Z' = -1000F_3/(\rho L^2U^2/2)$ Vertical force

$M' = -1000F_5/(\rho L^3U^2/2)$ Pitching moment

L	Length of the body
U	Forward speed
ρ	Water density
α	Angle of attack

CONCLUSIONS

The computed forces and moments of non-body-of-revolution hulls with angle of attack are compared with the experimental data. The agreement between the prediction and experiment is excellent for the UUV and SUBOFF. The computed forces and moments for the non-body-of-revolution hulls with elliptical sections are compared with those of the body of revolution. With the same separation angles for the body of revolution, the forces for a flat body are computed smaller than those of the body of revolution and the moments are computed larger than those of the body of revolution. The forces for a slender body are computed larger than those of the body of revolution and the moments are computed smaller than those of the body of revolution. An experiment for the non-body-of-revolution hull with elliptical sections is necessary to validate the present method. To extend the present method for other non-body-of-revolution hulls, the information about the separation line is also vital.

ACKNOWLEDGMENTS

The author acknowledges the support of Dr. I. Koh. He also likes to thank Dr. Edward Ammeen and Mr. Kurt Junghans for providing technical guidance.

REFERENCES

1. Hong, Y.S., "Computation of the Hydrodynamic Forces and Moments on a Body of Revolution With and Without Appendages," David Taylor Research Center Report DTRC/SHD-1003-06 (August 1991)
2. Meier, H.U. and H-P. Kreplin, "Experimental Investigation of the Transition and Separation on a Body of Revolution," Second Symposium on Turbulent Shear Flow, July 2-4, 1979, London.
3. Hess, J.L. and A.M.O. Smith, "Calculation of Non-lifting Potential Flow about Arbitrary Three-dimensional Bodies," Douglas Aircraft Co., Inc., Report No. E.S. 4062 (March 1962)
4. Roddy, R.F. and Dempsey, E., "Investigation of the Stability and Control Characteristics of the Rockwell Vehicle from Captive Model Experiments," Naval Surface Warfare Center, Carderock Division Report CRDKNSWC-HD-1391-02, February 1993
5. Roddy, R.F., "Investigation of the Stability and Control Characteristics of Several Configurations of the DARPA SUBOFF Model (DTRC Model 5470) from Captive-Model Experiments," David Taylor Research Center Report DTRC/SHD-1298-08, September 1990

Table 1. Principal dimensions

	UUV	SUBOFF	CFF1	CFF2
Length L, m (ft)	9.093 (29.833)	4.356 (14.292)	4.356 (14.292)	4.356 (14.292)
Width B, m (ft)	1.829 (6.0)	0.508 (1.666)	0.622 (2.041)	0.415 (1.361)
Height H, m (ft)	1.829 (6.0)	0.508 (1.666)	0.415 (1.361)	0.622 (2.041)

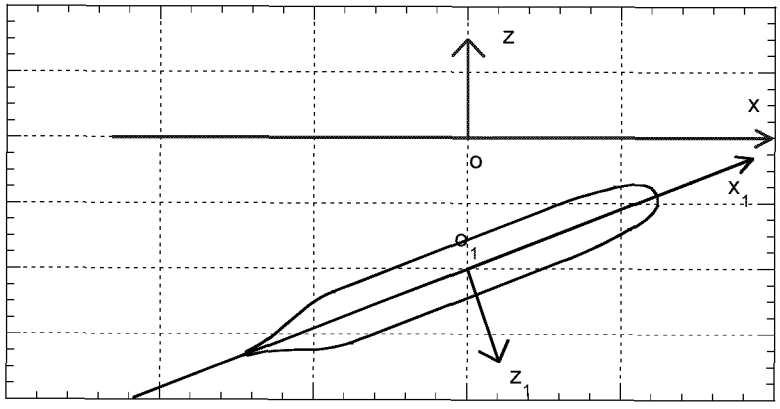

Fig. 1. Coordinate system

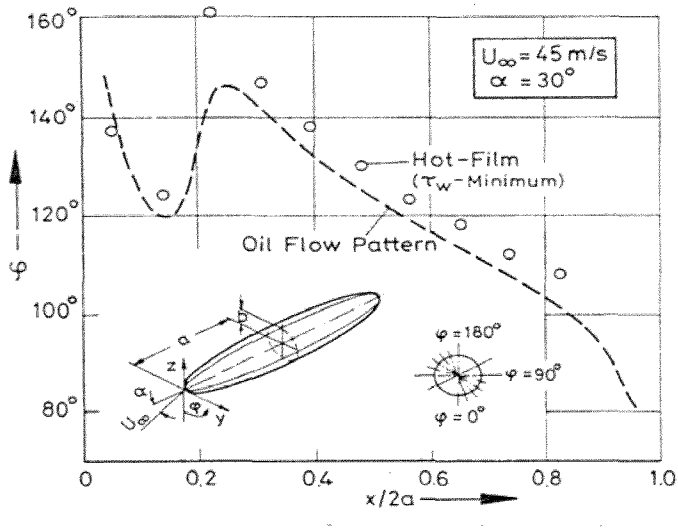

Fig 2. Separation angle for a spheroid with a length to diameter ratio of 6 for angle of attack of 30 degrees (Ref. 2)

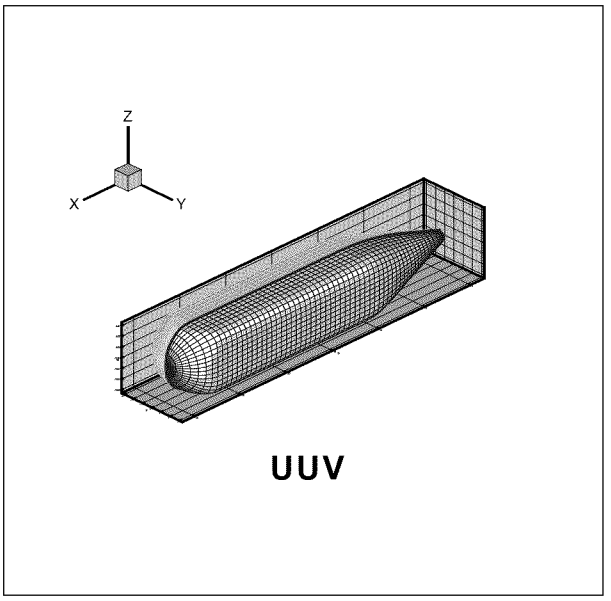

(a) UUV

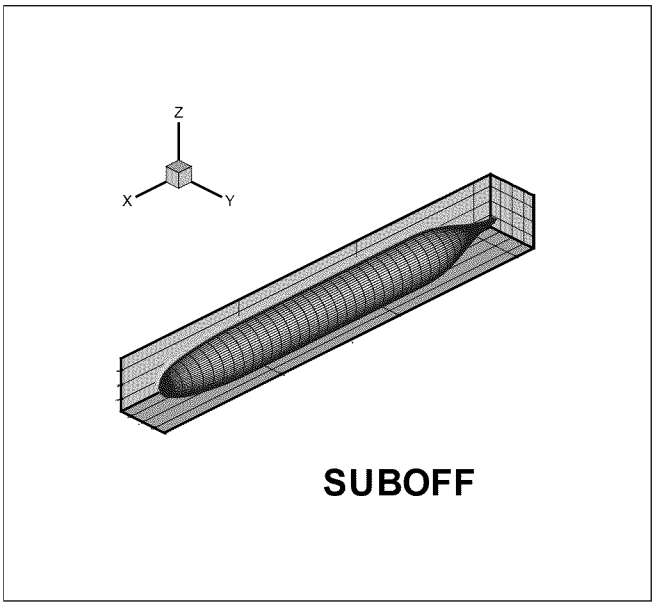

(b) SUBOFF

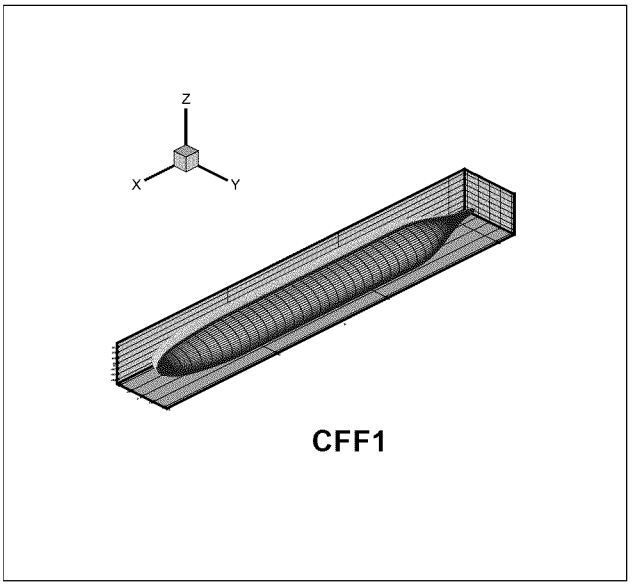

(c) CFF1

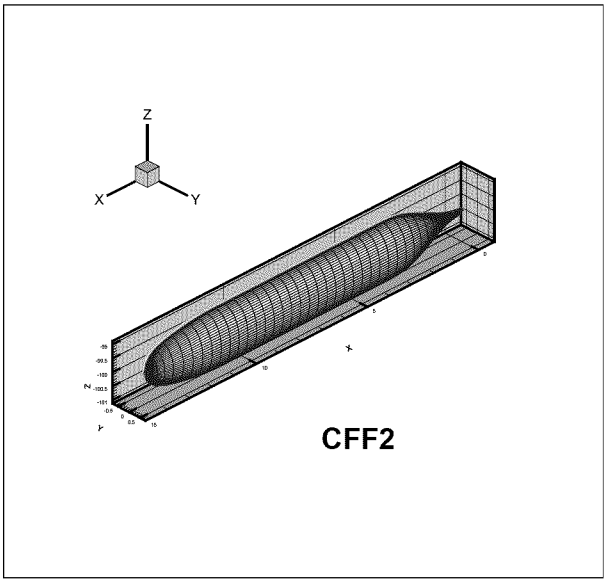

(d) CFF2

Fig. 3. Discretized body surface

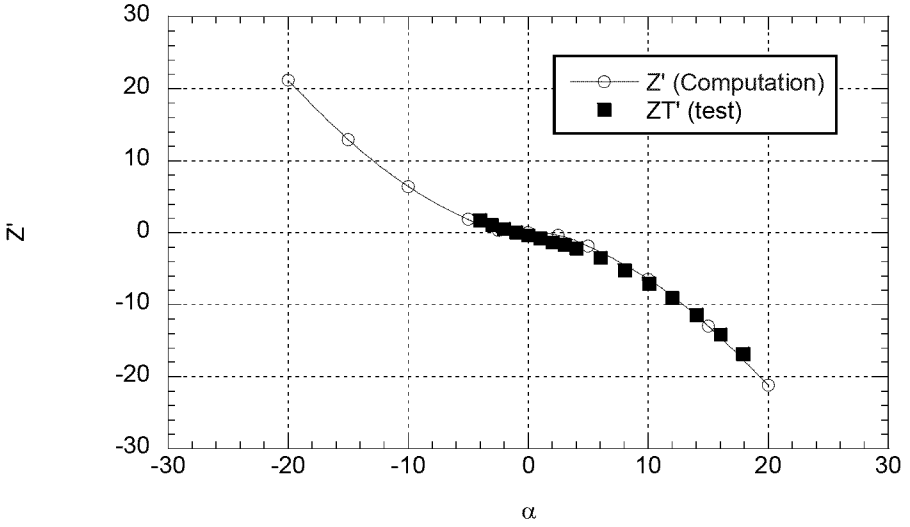

(a) Vertical force

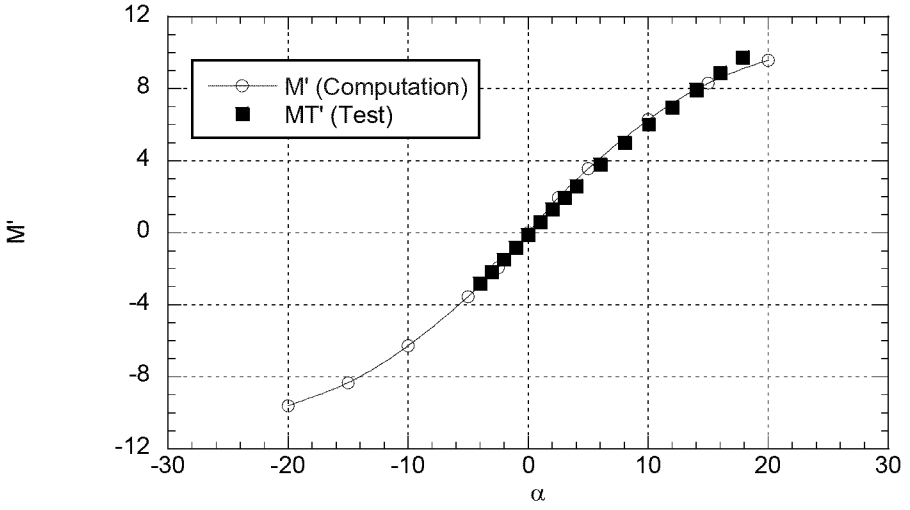

(b) Pitching moment

Fig. 4. Vertical forces and pitching moments of UUV

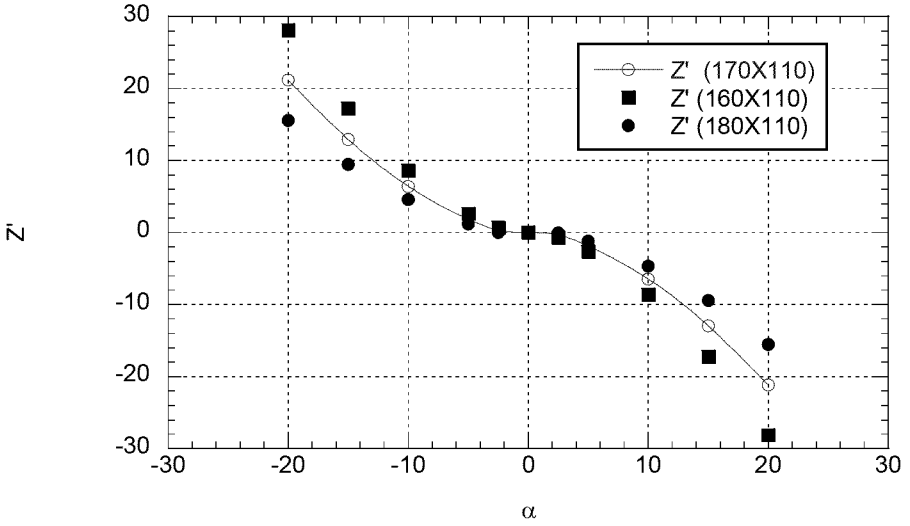

(a) Vertical force

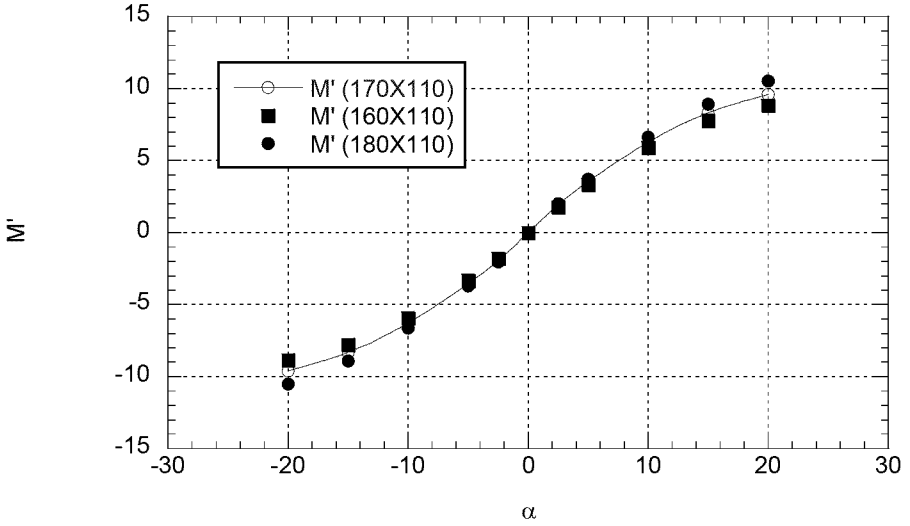

(b) Pitching moment

Fig. 5. Vertical forces and pitching moments of UUV for the different separation angles at the bow

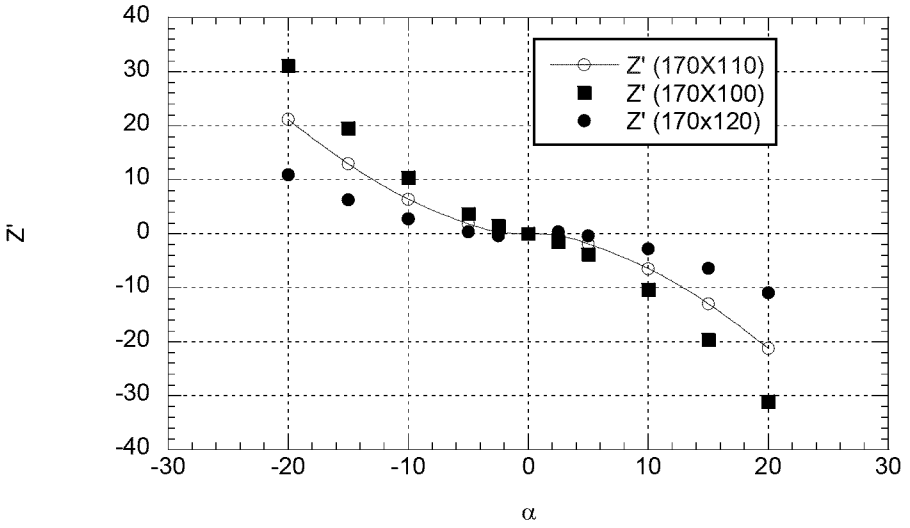

(a) Vertical force

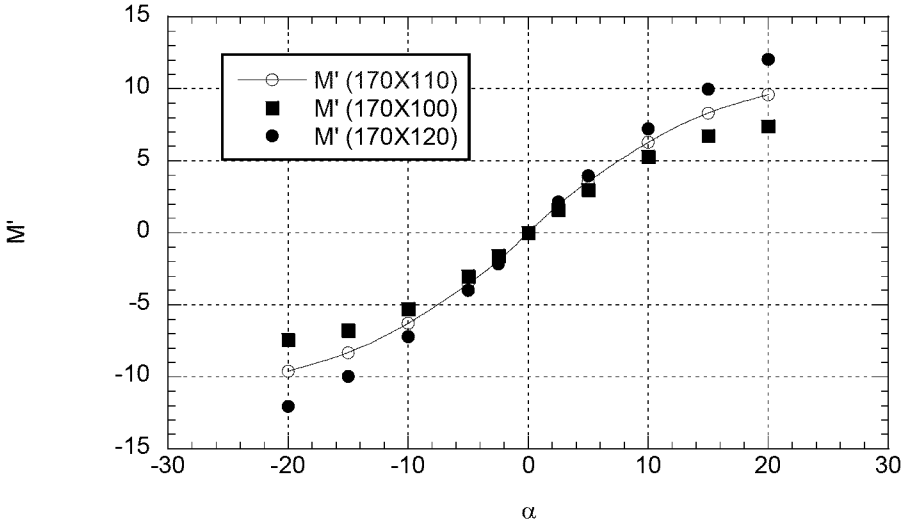

(b) Pitching moment

Fig. 6. Vertical forces and pitching moments of UUV for the different separation angles at the stern

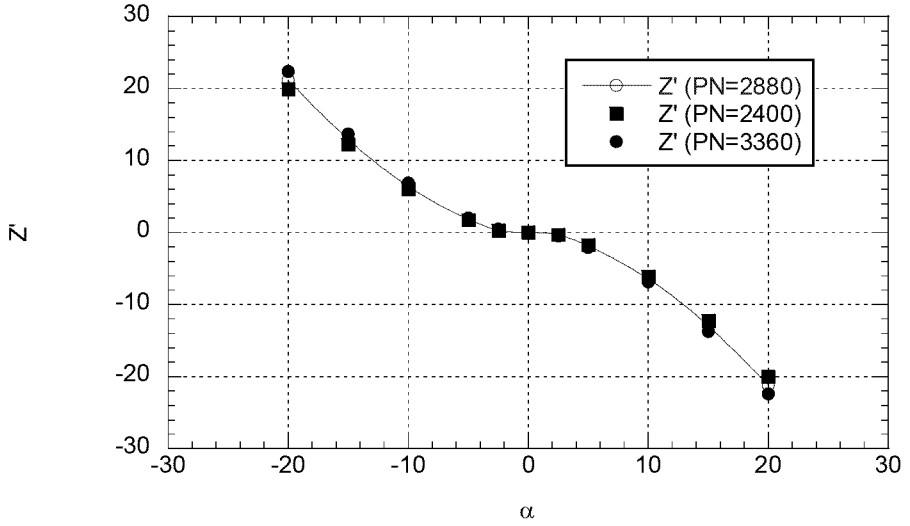

(a) Vertical force

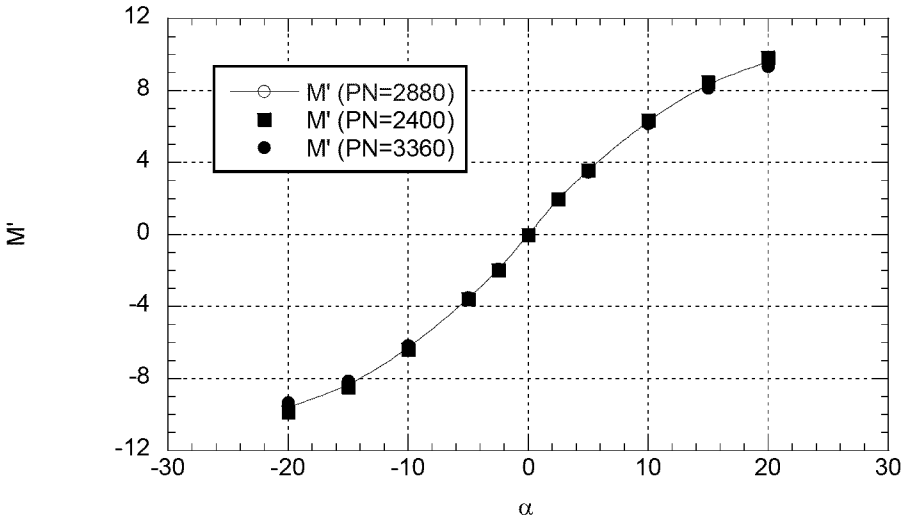

(b) Pitching moment

Fig. 7. Vertical forces and pitching moments of UUV for the different numbers of surface elements

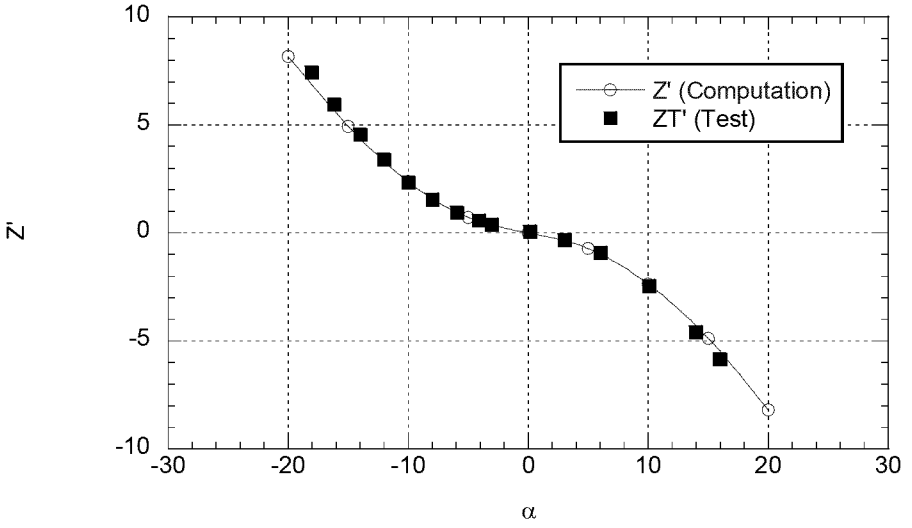

(a) Vertical force

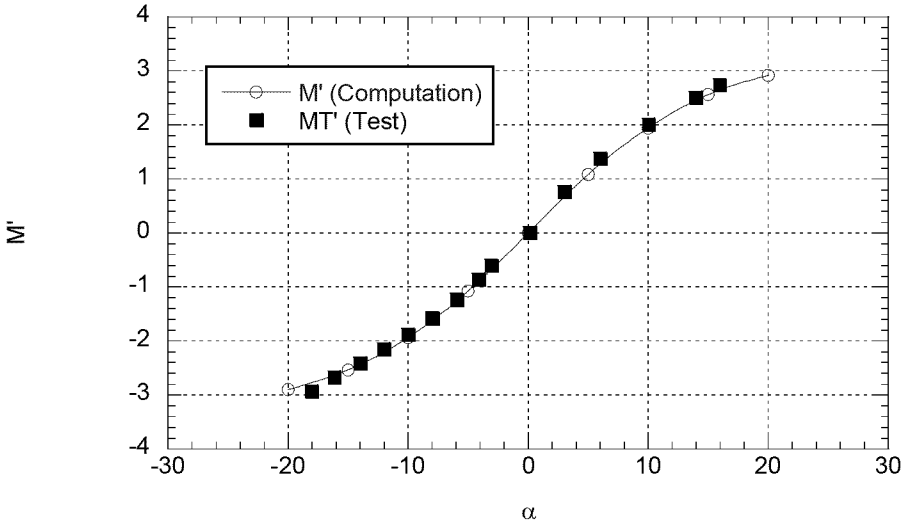

(b) Pitching moment

Fig. 8. Vertical forces and pitching moments of SUBOFF

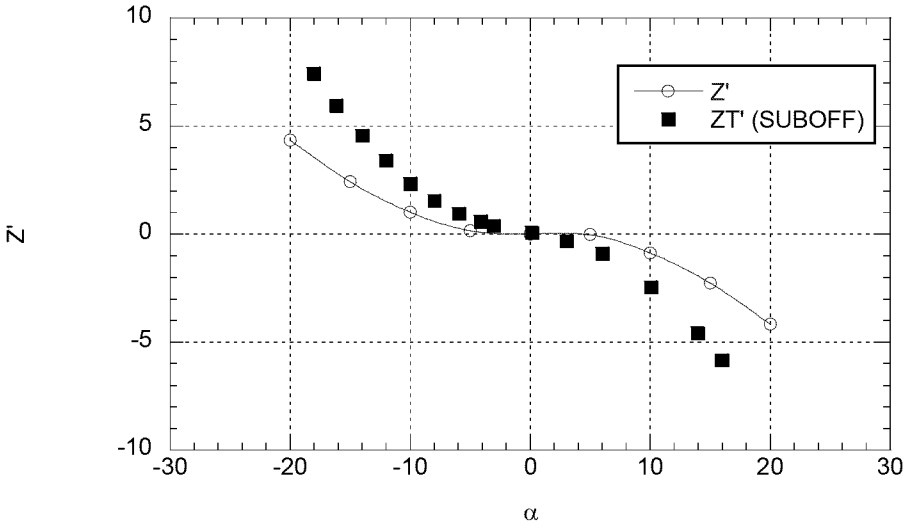

(a) Vertical force

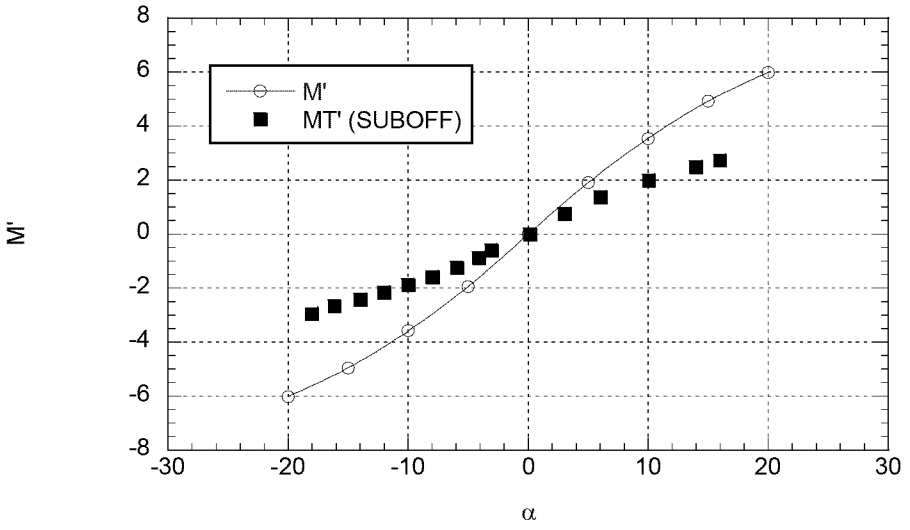

(b) Pitching moment

Fig. 9. Vertical forces and pitching moments of CFF1

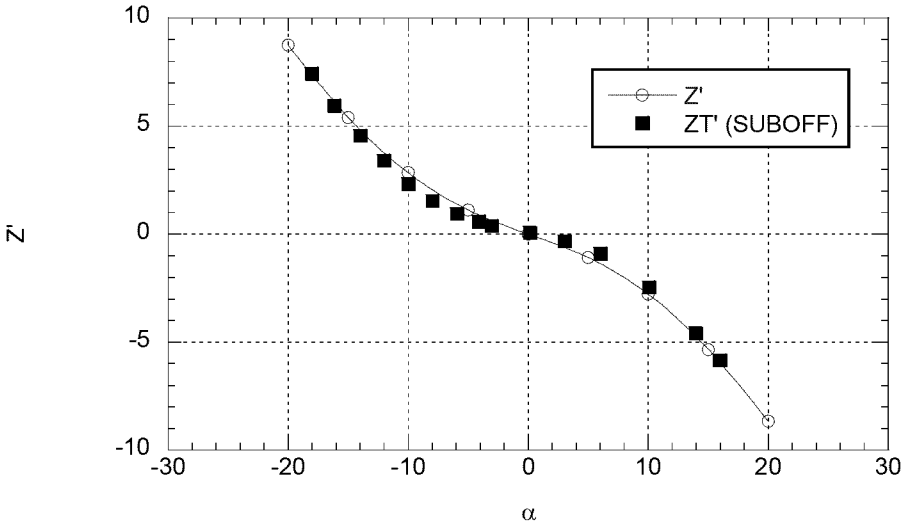

(a) Vertical force

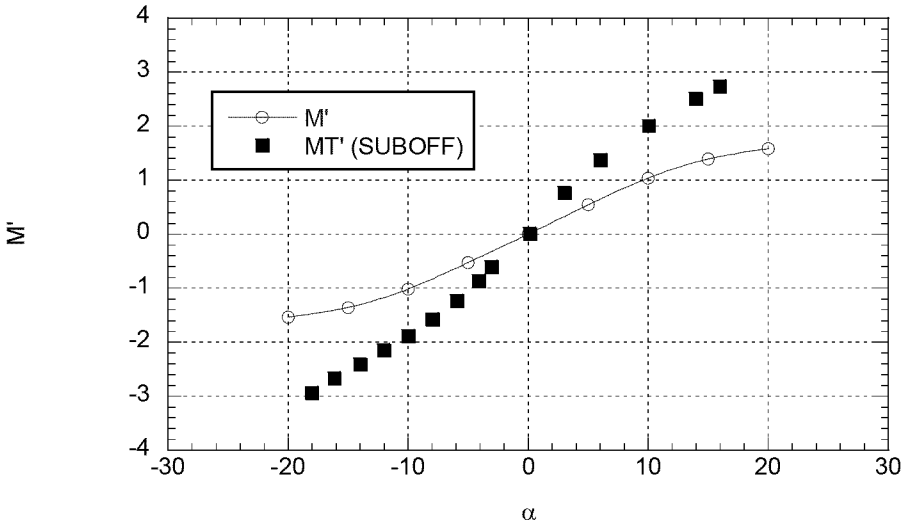

(b) Pitching moment

Fig. 10. Vertical forces and pitching moments of CFF2